

Chapter 2

Metal Injection Molding (MIM) Processing

Hideshi Miura, Toshiko Osada, and Yoshinori Itoh

Abstract Complex-shaped components can be obtained by net or near-net shaping through the powder metallurgy processing route such as metal injection molding (MIM) process. MIM is an advanced powder processing technique for the mass production of complex-shaped components. This technology also reduces the material used for production and processing cost. Sintered compacts obtained by MIM process show high density over 95 % and excellent mechanical properties. Titanium and its alloys are used in biomedical applications because of their excellent characteristics such as high specific strength, corrosion resistance, biocompatibility, and so on. MIM process is a suitable technique for titanium and its alloys to reduce the processing cost and material cost. In this chapter, tensile and fatigue properties of MIM compacts fabricated with Ti, Ti-6Al-4V, Ti-6Al-4V-4Cr, and Ti-6Al-7Nb are reviewed.

Keywords MIM process • Net shape • Tensile strength • Fatigue limit • Microstructure • Oxygen content • Titanium alloys

2.1 Introduction

Metal injection molding (MIM) combines the most useful characteristics of powder metallurgy (PM) and plastic injection molding to facilitate the production of small, complex-shaped metal components with outstanding mechanical properties.

Injection molding is a productive and widely used technique for shaping plastics. Alternatively, metals have advantages over polymers in mechanical properties and electrical and thermal conductivity. PM also has advantages such as easy alloying by powders and recycle ability. MIM uses the metal powder and binder plastics; thus, this is a combined process of injection molding and PM.

H. Miura (✉) • T. Osada
Department of Mechanical Engineering, Kyushu University, 744 Motooka, Nishi-ku,
Fukuoka 819-0395, Japan
e-mail: miura@mech.kyushu-u.ac.jp

Y. Itoh
Hamamatsu Industrial Research Institute of Shizuoka Prefecture, 1-3-3, Shinmiyakoda,
Kita-ku, Hamamatsu, Shizuoka 431-2103, Japan

This chapter introduces the MIM process and provides the tensile and fatigue properties of various injection molded titanium alloy compacts.

2.2 Metal Injection Molding

2.2.1 MIM Process

Metal injection molding (MIM) is an advanced manufacturing technology that uses the shaping advantage of injection molding process to be applied to metal. The process has ability to produce the high degree of geometrical complexity of the component with high properties. Because of high final density, often near theoretical density, the MIM products exhibit excellent properties. MIM process is applicable for most of common engineering metals such as carbon steel, stainless steel, tungsten, nickel-based alloys, titanium alloys, etc. Figure 2.1 shows the advantages of the MIM process [1]. MIM has been demonstrated to be a cost-effective manufacturing process of small components (typically less than 50 g for titanium alloys), complex-shaped parts with high production volume, as it can be seen in Fig. 2.2.

The principle of the MIM process is illustrated in Fig. 2.3. Initially, powder and thermoplastic binder are mixed and kneaded in order to obtain the feedstock. This feedstock is heated and injected into a mold using a conventional injection molding machine. After the injection process, the binder is removed by heating, chemical extraction, or catalytic reaction, and then this is followed by sintering process to produce the final parts. The binder removal process is called the debinding process.

The purpose of sintering is to densify the powder and to remove most of the void space left by the binders. Usually the shrinkage during sintering is in the range between 12 and 18 %; therefore, the mold is oversized to meet the required dimension. The MIM component has tolerance ranging from ± 0.05 to ± 0.3 %.

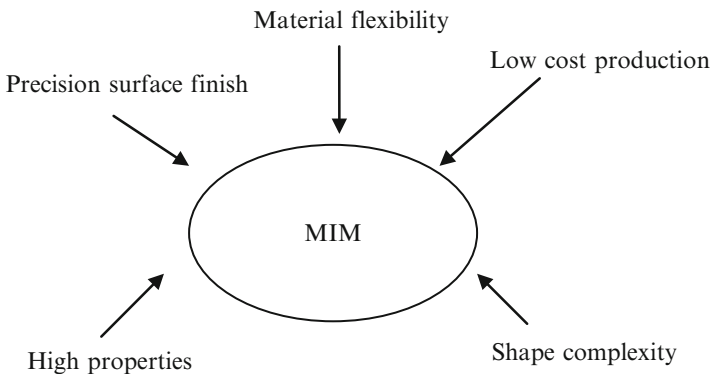


Fig. 2.1 The advantages of MIM process (Redrawn from Ref. [1])

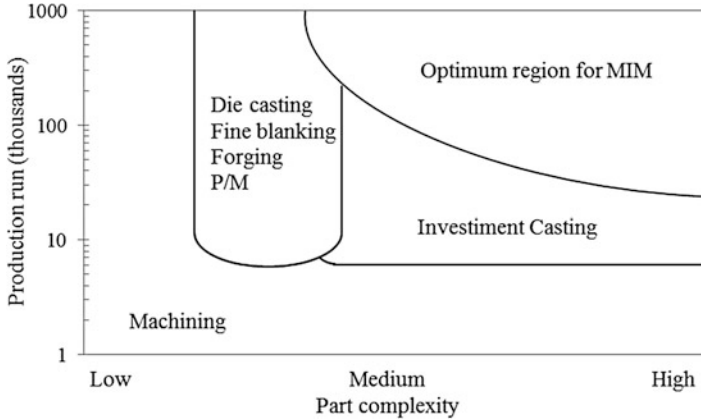


Fig. 2.2 MIM is suited to complex-shaped parts with high production volume (Redrawn from Ref. [1])

After sintering process, the secondary operations such as grinding, machining, and drilling can be omitted. However, it depends on the accuracy of the product. For the mechanical parts, which need tighter tolerance, an approach to achieve tighter tolerance is to machine the critical surface after sintering. Hence, it is only applied for critical features. Surface roughness depends on the tools and also powder size. After sintering process, the sand blasting process can be done to reduce the surface roughness.

Another point is in the MIM process; the feedstock material can be recycled nearly 100 %. This will be beneficial for cost reduction, especially for the expensive materials. The total cost of binders, mold, debinding, and sintering process can be reduced by increasing the amount of production. In other words, the low cost of MIM process is suitable for the mass production. The summary of this section is that, with the capability of producing complex-shaped component with high properties at low cost, MIM process is expected to be one of the suitable processes to fabricate complex biomedical parts.

2.2.2 Biomedical Applications

MIM is suitable for the fabrication of small and complex-shaped parts; thus, several parts for medical applications were produced. Figure 2.4 shows the examples of biomedical components [3–7]. Those are fabricated from stainless steel, Ti alloy, and so on.

MIM is a very clean process compared to conventional manufacturing technologies. Only the possible binder residuals could represent potential candidates as

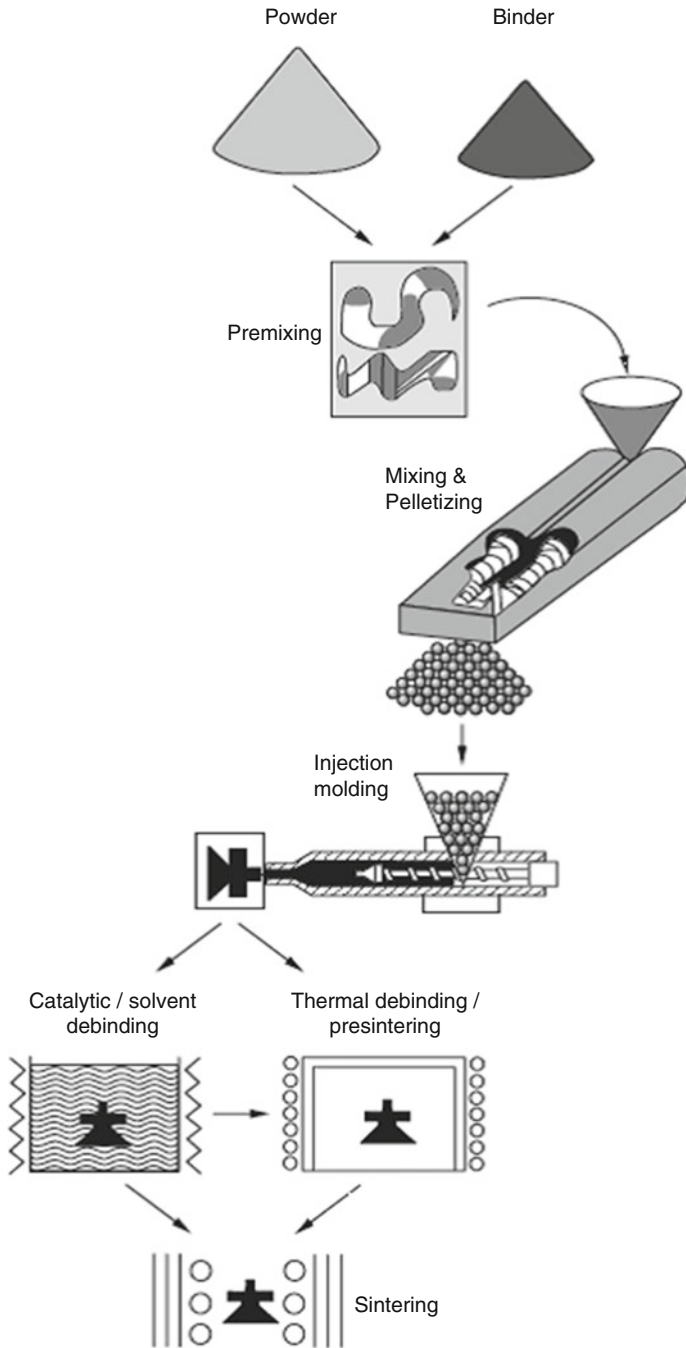


Fig. 2.3 Schematic diagram of MIM process (Reproduced with permission from Ref. [2]. Copyright 1996, Uchida Rokakuho Publishing Co., Ltd.)



Fig. 2.4 MIM products for biomedical applications. (a) Orthodontic parts, SUS630, Ti, Al_2O_3 ; (b) surgical scalpel holder, SUS630; (c) fracture fixation plate, SUS316L; (d) heart valve, titanium; (e) an implant pump, Ti-6Al-4V; (f) dental implant, titanium

toxic substances [8]. It is a good start to use exclusively nontoxic biocompatible binder components. Even if the single binder constituents may be harmless, such as paraffin or polyethylene, decomposition at high temperature could generally lead to new toxic substances. However, these substances would be trapped in pores after sintering and would cover the surface. In the first instance, they would have no contact with the body, and in the latter case, they could be removed if necessary. In the end, appropriate tests of the sintered components have to prove this.

MIM for the fabrication of medical implants is also interesting because of the possibility of generating porous components. These are beneficial with regard to

tissue ingrowth. Porosity and pore diameter could be easily controlled. Figure 2.4f shows the implant that has a dense layer covered by a porous layer.

2.2.3 Titanium Alloys Fabricated by MIM

Ti and its alloys show excellent characteristics of low density, high strength, and high biocompatibility, leading to their widespread use for various industrial and biomedical applications. However, they show poor workability, so it is difficult to use them to produce parts with complicated shapes at low processing cost. Therefore, MIM process is a suitable technique for fabricating the complex-shaped parts to reduce the processing cost and material cost. Ti-6Al-4V is well known as the most widely used Ti-based alloy. Meanwhile, MIM can be used to produce various types of Ti alloys using mixed powders [8, 9].

As shown in Fig. 2.4, MIM is favored by a large number of small complex parts. Cosmetic parts had been successfully made from CP Ti powder, but for the structural applications, the oxygen level is still high especially for Ti-6Al-4V alloy. Nowadays, the oxygen content of Ti-6Al-4V products can be controlled to about 0.2 mass% with low oxygen level of starting powders, development of binders, and sintering facilities. This development promises a significant expansion of the titanium MIM marketplace into aerospace, automobiles, surgical instruments, dentistry, and so on.

2.3 Static Mechanical Properties of Ti Alloys Fabricated by MIM

In this section, the properties of injection molded Ti-6Al-4V alloy compacts using alloy powders and various mixed powders were investigated comprehensively to clarify the effect of oxygen content and relative density on the tensile properties.

On the other hand, Ti-6Al-7Nb alloy has been developed for more suitable biomaterial in place of Ti-6Al-4V alloy, because the vanadium (V) is toxic to the human body. There are few reports about MIM Ti-6Al-7Nb alloy, though the cost of starting material powder seems to be expensive because of not using a commercially available powder of gas-atomized Ti-6Al-7Nb alloy powder [10] or Al-53.8Nb pre-alloyed powder [11].

In this section, the metal injection molding process of Ti-6Al-7Nb alloy using an alloy powder and three types of mixed powders, which consisted of commercially available powders, is reviewed. The effects of powders and sintering conditions on the microstructure, relative density, and mechanical properties of injection molded compacts were mainly investigated.

Table 2.1 Chemical composition and mean particle diameter of the powders

		Chemical composition (mass%)					Particle diameter (μm)
		Al	V	Fe	O	C	
Ti		–	–	0.044	0.130	0.008	24.4
Ti-6Al-4V		5.75	4.13	0.017	0.100	0.004	26.1
TiH ₂		–	–	0.03	0.170	–	15.0
Al-40 V	Fine	Bal.	41.0	0.24	0.47	0.02	6.4
	Coarse	Bal.	39.7	0.33	0.20	0.01	20.0
	Atomized	59.5	Bal.	0.13	0.12	0.02	26.0

2.3.1 Effect of Oxygen Content in Ti-6Al-4V Compacts

2.3.1.1 Experimental Procedures

A gas-atomized pure Ti powder (TILOP-45, Osaka Titanium Technologies Co., Ltd.), ground TiH₂ powder with a different particle diameter and shape (TCH452, Toho Titanium Co., Ltd., etc.), two types of ground Al-40V alloy powders with different particle diameters (VAL-3, Nippon Denko Co., Ltd.), gas-atomized Al-40V alloy powder (60Al-40V, Daido Steel Co., Ltd.), and three types of Ti-6Al-4V alloy powders with different particle diameters and oxygen contents (TILOP64-45, Osaka Titanium Technologies Co., Ltd., etc.) were used in the experiment. The chemical compositions, particle diameter, and scanning electron microscope (SEM) images of these powders are shown in Table 2.1 and Fig. 2.5. The TiH₂ powder is more cost-effective compared with gas-atomized Ti powder, which should reduce raw material costs [12]. The fine Al-40V powder shows higher oxygen content than the other Al-40V powders.

The pure Ti powder, TiH₂ powder, and Al-40V alloy powder were weighed to obtain the chemical composition of Ti-6Al-4V and then were premixed for 3.6 ks by rotating in an argon gas-filled pot mill. The mixtures of Ti-6Al-4V alloy powder were then kneaded with binder [13] (which contained polypropylene, polymethyl methacrylate, paraffin wax, and stearic acid in a weight ratio of 30:40:29:1) using a pressure-type kneading machine (Moriyama Co., Ltd., DV1-5GHH-E) at 443 K for 8.1 ks. The binder loading was 35 vol%, and it increased with increasing TiH₂ powder content because of its irregular shape and low density. The compounds obtained were crushed and screened from 2 to 8 mm diameter to prepare feedstocks for injection molding. The feedstocks were then injection molded by injection molding machine (Nissei Plastic Industrial Co., Ltd., ST20S2V) to produce tensile test specimens with a length of 75 mm, a width of 5 mm, and a thickness of 2 mm. After injection molding, solvent extraction debinding was conducted at 343 K for 21.3 ks in *n*-hexane [13] to partially remove the wax and polymethyl methacrylate. By this treatment, the contamination of sintered compacts by carbon derived from the binder system was reduced. Following this treatment, thermal debinding was performed from room temperature to 703 K in reduced pressure under argon gas flow. Continuous sintering was performed in high vacuum (in the order of below 10^{-2} Pa) at various temperatures for 3.6 to 28.8 ks, followed by furnace cooling to

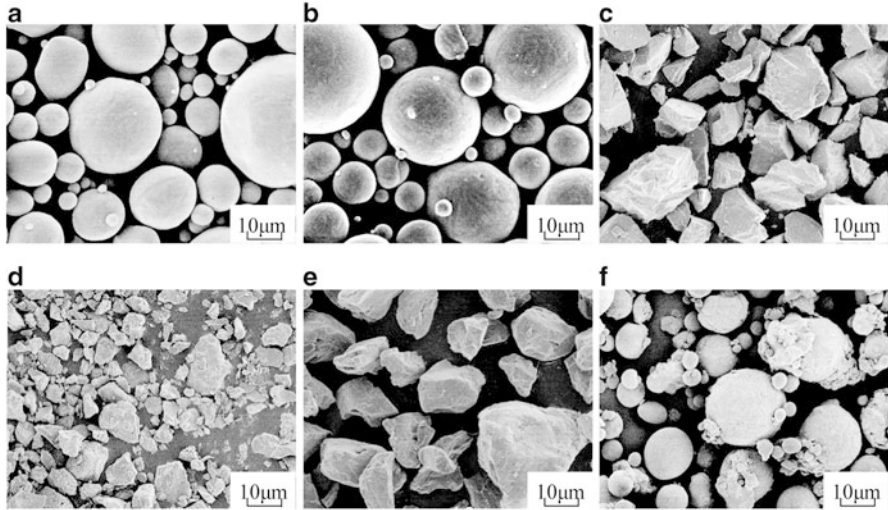


Fig. 2.5 SEM images of (a) titanium powder, (b) Ti-6Al-4V alloy powder, (c) titanium hydride (TiH_2) powder, (d) fine Al-40V alloy powder, (e) coarse Al-40V alloy powder, and (f) atomized Al-40V powder

room temperature in high vacuum (in the order of below 10^{-3} Pa). The vacuum furnace (Shimadzu Mectem Inc., PVSGgr20/20) has both its heater elements and vessel made from graphite. The compacts were set on yttria or zirconia substrates in an inner vessel made from molybdenum or zirconia, and the compacts were surrounded by a spongelike Ti powder to prevent their carburization and oxidation.

The relative densities and tensile properties were measured on as-sintered compacts. The density of sintered compacts was measured by the Archimedeian method with an automatic densimeter (Toyo Seiki Seisaku-Sho, Ltd., DENSIMETER H), and the relative density was calculated against the full density of Ti-6Al-4V alloy (4.42 Mg/m^3). The tensile testing (in triplicate) was conducted using a universal testing instrument (Shimadzu Corp., AG-50kNIS) with an extensometer gauge length of 25 mm and crosshead speed of $8.33 \times 10^{-5} \text{ m/s}$ in air at room temperature. The oxygen content was determined by means of Oxygen/Nitrogen analyzer (Horiba, Ltd., EMGA-520).

2.4 Results and Discussion

Table 2.2 shows the typical properties of sintered Ti-6Al-4V alloy compacts discussed in this section. For details of these properties, refer to previous papers [12, 14–18].

The relative density of the compacts using a mixture of Ti, TiH_2 , and Al-40V alloy powders increased with increasing TiH_2 content. At the same time, the

Table 2.2 Characteristic properties of sintered Ti-6Al-4V alloy compacts

Powder	Sintering condition	Vessel/ substrate	Relative density	Tensile strength	Elongation (%)	Oxygen content (%)
Ti, TiH ₂ , and coarse Al-40 V	1,373 K X 28.8 ks	Mo/ Y ₂ O ₃	98.3	990	4.9	0.41
		ZrO ₂ / ZrO ₂	98.5	930	15.8	0.35
Ti and fine Al-40v	1,473 K X 28.8 ks	Mo/ ZrO ₂	98.5	890	9.6	0.35
		ZrO ₂ / ZrO ₂	97.7	880	14.5	0.27
Ti and coarse Al-40v	1,373 K X 28.8 ks	Mo/ Y ₂ O ₃	98.4	820	13.7	0.24
Ti and atom-ized Al-40 V	1,473 K X 14.4 ks		96.7	790	12.3	0.20
Ti-6Al-4V ELI	1,423 K X 28.8 ks		96.4	760	11.0	0.18

powder loading of compacts decreased with increasing TiH₂ content because more binder was required to obtain enough flowability in the feedstock for injection molding. The tensile strength and oxygen content of the compacts using a mixture of Ti, TiH₂, and Al-40V alloy powders increased with increasing TiH₂ content. On the other hand, the elongation of the compacts using a mixture of Ti, TiH₂, and Al-40V alloy powders reduced drastically with increasing TiH₂ content [12].

The sintered compacts using a mixture of Ti and fine irregular Al-40V alloy powder showed the highest density, and the compacts using a mixture of Ti and coarse, irregular Al-40V alloy powder showed slightly higher density than the compacts using a mixture of Ti and spherical atomized Al-40V alloy powder. The sintered compacts using a mixture of Ti and fine irregular Al-40V alloy powder, which had the highest oxygen content compared with other Al-40V alloy powders, showed high oxygen content [14, 18]. Furthermore, the molybdenum vessel and yttria substrate could be effective to oxidation of the compacts from sintering atmosphere [15], which resulted in enough ductility, even for the prolonged sintering time at high sintering temperature to obtain high density.

The sintered compacts using Ti-6Al-4V alloy powders showed slightly lower relative density compared with the compacts using mixed powders, and their tensile properties were slightly low [16]. However, they were improved by prolonged sintering time and higher sintering temperature or using a small particle size powder [17]. The oxygen content of the sintered compacts using a Ti-6Al-4V ELI (extra-low interstitial) powder reached below 0.2 mass% as shown in Table 2.1 and Table 2.2.

The relative density and oxygen content of the compacts in our previous studies cover a wide range from 90 to 99.8 % and 0.18 to 0.85 mass% O, respectively. As shown in Table 2.2, there is a tendency for the tensile strength of sintered compact to decrease with increasing oxygen content.

Fig. 2.6 Effect of oxygen content on the elongation of Ti-6Al-4V alloy compacts sintered under various conditions with various mixed or Ti-6Al-4V alloy powders

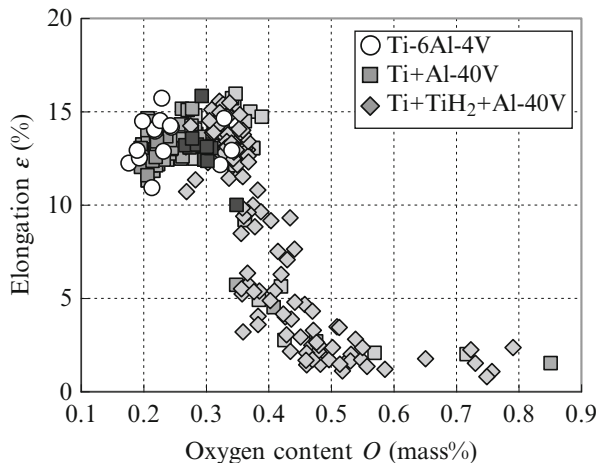


Figure 2.6 shows the effect of oxygen content on the elongation of sintered Ti-6Al-4V alloy compacts using various mixed powders or Ti-6Al-4V alloy powder. The tensile properties of the compacts with relative density below 94.5 % were excluded because of their poor properties and large fluctuation. The elongation of the compacts using any mixed powder or Ti-6Al-4V alloy powder and also any sintering conditions shows the excellent values, in excess of 10 %, when the oxygen content of the sintered compacts is below 0.35 mass%. However, the elongation of the sintered compacts is reduced dramatically if the oxygen content exceeds 0.35 mass%.

Figure 2.7 shows the effect of oxygen content on the elongation of sintered Ti-6Al-4V alloy compacts as a function of relative density for the oxygen content range from 0.1 to 0.35 mass%. The solid line shows the effect of oxygen content on the elongation of sintered Ti-6Al-4V alloy compacts which have relative densities from 97.5 to 98.5 %, as an approximated line. The oxygen content of sintered Ti-6Al-4V alloy compacts has little influence on the elongation when the sintered compacts have ductility greater than 10 % elongation. In addition, the relative density of sintered Ti-6Al-4V alloy compacts has very little influence on the elongation from the result of approximated line calculated for each relative density range.

Figure 2.8 shows the effect of oxygen content on the tensile strength of sintered Ti-6Al-4V alloy compacts using various mixtures of Ti-6Al-4V alloy powder. The tensile strength of the compacts using any mixed powder or Ti-6Al-4V alloy powder and also any sintering condition increases from approximately 800 to 1,000 MPa with increasing oxygen content below 0.5 mass%, but they are drastically reduced from the oxygen content above 0.5 mass%.

Figure 2.9 shows the effect of oxygen content on the tensile strength of sintered Ti-6Al-4V alloy compacts as a function of relative density in the oxygen content range from 0.1 to 0.5 mass%. The solid line and light solid line show the effect of oxygen content on the tensile strength of sintered Ti-6Al-4V alloy compacts with relative densities from 98.5 to 99.5 % and from 94.5 to 95.5 % as an approximated line, respectively. From the difference among each line, the tensile strength of sintered Ti-6Al-4V alloy compacts is improved by 40 MPa with increasing 4 % of

Fig. 2.7 The relationship between the oxygen content under 0.35 mass% and the elongation of Ti-6Al-4V alloy compacts sintered by various conditions with various mixed or Ti-6Al-4V alloy powders

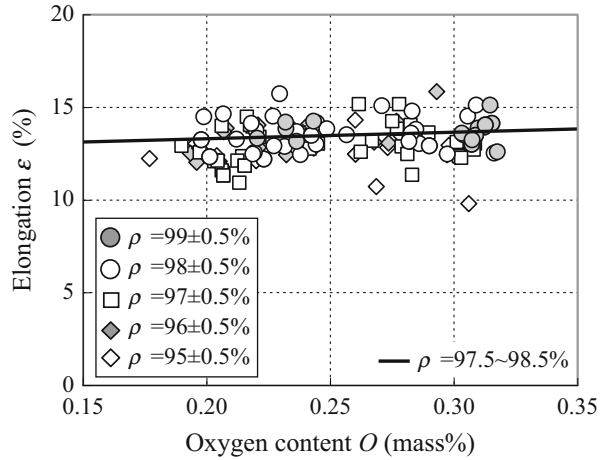
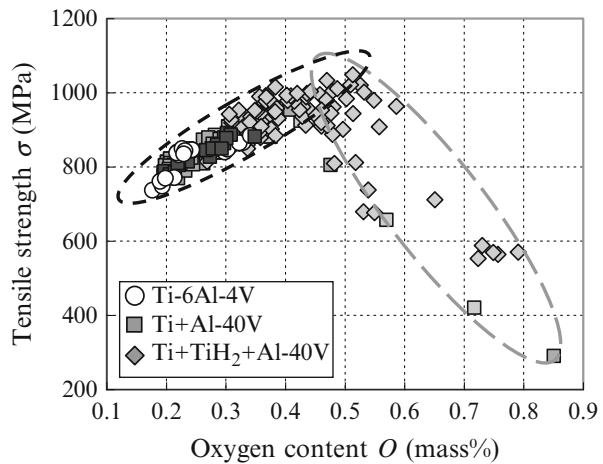


Fig. 2.8 Effect of oxygen content on the tensile strength of Ti-6Al-4V alloy compacts sintered by various conditions with various mixed or Ti-6Al-4V alloy powders



relative density. Furthermore, from the slope of each line, the tensile strength of sintered Ti-6Al-4V alloy compacts is improved by 70 MPa with each increasing 0.1 mass% O. In other words, it was found that the tensile strength of sintered Ti-6Al-4V alloy compacts is greatly affected by oxygen content and relative density of the compacts. From these results, the tensile strength (σ) of sintered Ti-6Al-4V alloy compacts shows an excellent correlation with oxygen content (O) and relative density (ρ) as shown in the following experimental Eq. (2.1):

$$\sigma(\text{MPa}) = 700O(\text{mass}\%) + 10\rho(\%) - 315 \quad (2.1)$$

(Provided that $O < 0.5$ mass% and $\rho > 94.5$ %)

To confirm the viability of experimental Eq. (2.1), the comparison was made between calculated tensile strength and experimental values. Figure 2.10 shows the effect of relative density and oxygen content on the tensile strength of Ti-6Al-4V

Fig. 2.9 The relationship between the oxygen content and the tensile strength of Ti-6Al-4V alloy compacts sintered under various conditions with various mixed or Ti-6Al-4V alloy powders

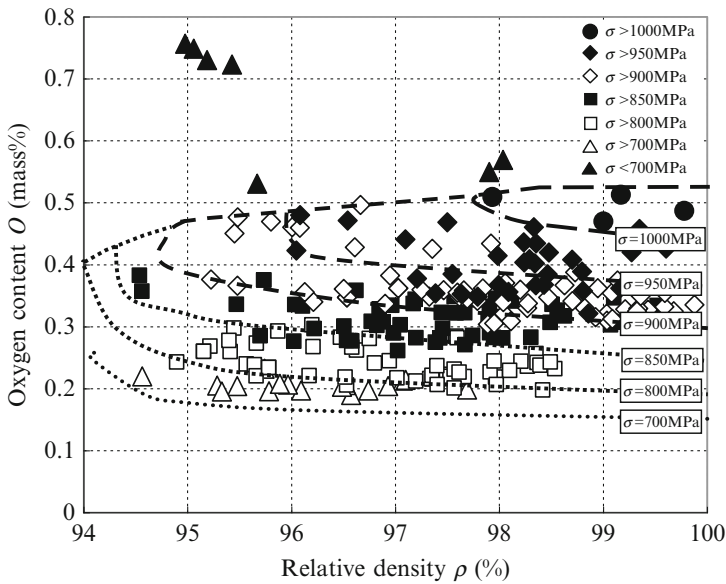
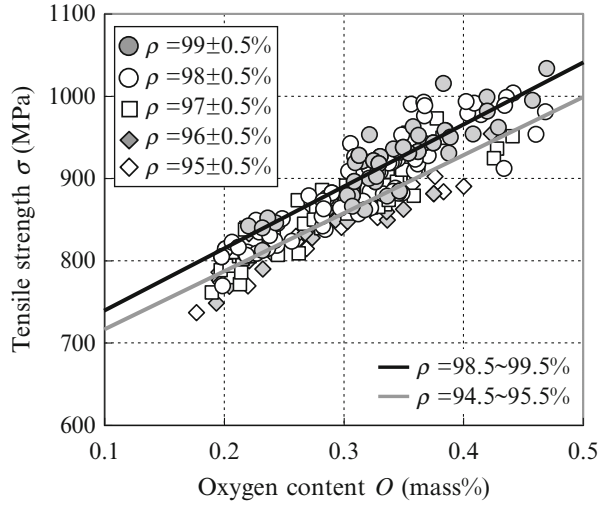


Fig. 2.10 Effect of the relative density and oxygen content on the tensile strength of Ti-6Al-4V alloy compacts sintered under various conditions with various mixed or Ti-6Al-4V alloy powders

alloy compacts sintered under various conditions with various mixed or Ti-6Al-4V alloy powders by plotting each experimental value and approximate contour lines. The highest strength sintered compacts are shown in the region of high oxygen and high relative density.

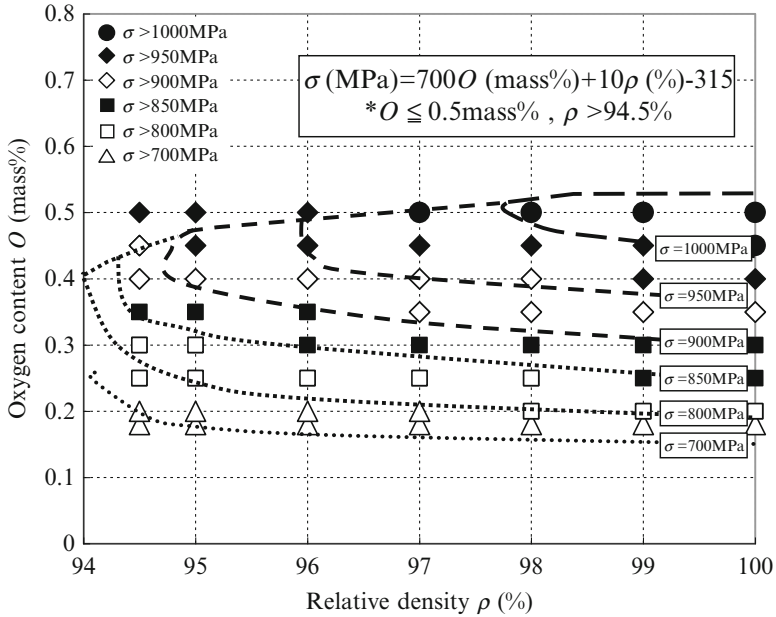


Fig. 2.11 The relationship between the calculated values and the experimental curved lines for tensile strength of sintered Ti-6Al-4V alloy compacts as a function of relative density and oxygen content

Figure 2.11 shows the relationship between calculated values and experimental contours (shown in Fig. 2.10) of tensile strength of sintered Ti-6Al-4V alloy compacts as a function of relative density and oxygen content (provided that oxygen is in the range 0.18–0.5 mass% and relative densities are in the range 94.5–100 %). The calculated values of tensile strength are in fair agreement with the experimental curved line. Thus, the correlation between the tensile strength of sintered Ti-6Al-4V alloy compacts and oxygen content and relative density can be expressed by the experimental Eq. (2.1).

2.4.1 Ti-6Al-7Nb

2.4.1.1 Experimental Procedure

Gas-atomized Ti-6Al-7Nb alloy and pure Ti (from Sumitomo Titanium Corp.), Nb (from Kojundo Chemical Laboratory Co., Ltd.), Ti-Al alloy (Ti-35.7Al, from KCM Corp.), Al-Nb alloy (Al-53.8Nb), and two types of Al powders with different particle diameters (from Minalco Co., Ltd.) were used. The chemical compositions and particle diameter of those powders are shown in Table 2.3, and a scanning electron microscope (SEM) image of Ti-6Al-7Nb alloy powder is shown in

Table 2.3 Chemical compositions and particle diameter of the powders used

Powder		Composition (mass%)			Particle diameter (μm)
		O	C	Fe	
Ti		0.140	0.008	0.044	<45
Al	Coarse	–	–	0.130	<45
	Fine	–	–	0.140	<10
Nb		–	–	0.004	<45
Ti-35.7Al		0.620	–	0.015	<45
Al-53.8Nb		0.064	0.024	–	<45
Ti-6Al-7Nb		0.157	0.023	0.083	<45

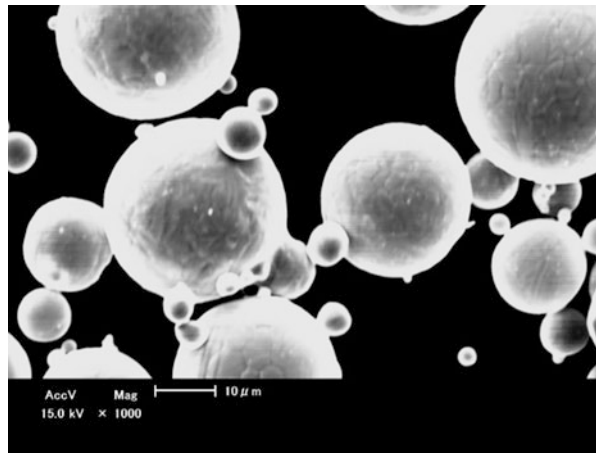
Fig. 2.12 SEM image of Ti-6Al-7Nb alloy powder

Fig. 2.12. The Ti-Al alloy powder shows higher oxygen content than Ti powder. Those powders were weighed to obtain the chemical compositions of Ti-6Al-7Nb and were premixed for 3.6 ks by pot mill rotator with argon gas-filled polyethylene pot. The powder mixtures were then kneaded with binder (which contained polypropylene, polymethyl methacrylate, paraffin wax, and stearic acid in a weight ratio of 30:40:29:1) by means of a pressure-type kneading machine (Moriyama Co., Ltd., DV1-5GHH-E) at 443 K for 8.1 ks. The powder loading was 65 vol.%. The compounds were molded by injection molding machine (Nissei Plastic Industrial Co., Ltd., ST20S2V) into compacts for tensile test specimen with a length of 75 mm, a width of 5 mm, and a thickness of 2 mm. After injection molding, the extraction debinding with vaporized solvent, which was conducted at 343 K for 21.3 ks in n-hexane, was used to partially remove the wax and polymethyl methacrylate. Following this treatment, thermal debinding was performed from room temperature to 703 K in reduced pressure with argon gas current, and continuous sintering was performed in vacuum (10^{-2} Pa order) at various temperatures for 14.4 ks, followed by furnace cooling. The vacuum furnace has both heater and vessel made from graphite, and the compacts were set on the yttria substrate in the Mo

vessel and were surrounded by a spongelike Ti powder. The relative density and tensile properties were measured on as-sintered compacts. The tensile test was conducted at a crosshead speed of 8.33×10^{-5} m/s in air at room temperature. The oxygen and carbon contents of sintered compacts were determined by means of Oxygen/Nitrogen analyzer (Horiba, Ltd., EMGA-520) and Carbon/Sulfur analyzer (Horiba, Ltd., EMIA-920 V). Microstructural observations of sintered compacts were conducted using an optical microscope. To determine the distribution of each element of sintered compacts, electron probe microanalysis was also performed.

2.4.1.2 Results and Discussion

Figure 2.13 shows the effect of sintering temperature on the relative density of Ti-6Al-7Nb compacts. The relative density of the compacts increases with increasing sintering temperature and reached up to 98 % and 97 % at 1350 °C, respectively, in contrast with 94 % for the compacts using a mixture of Ti, Nb, and coarse Al powders.

Figures 2.14 and 2.15 show the effect of sintering temperature on the oxygen and carbon contents of the Ti-6Al-7Nb alloy compacts. These values have sufficiently low level so that they do not have a detrimental effect on the mechanical properties of sintered compacts. The sintered compacts using a mixture of Ti, Nb, and Ti-Al powders have higher oxygen content derived from Ti-Al alloy powder, which suggests that there is difference in tensile properties between the sintered compacts using a mixture of Ti, Nb, and Ti-Al powders and using a mixture of Ti, Nb, and fine Al powders such as high tensile strength and low elongation.

The tensile properties of Ti-6Al-7Nb alloy compacts sintered at various temperatures are shown in Figs. 2.16 and 2.17. The tensile strength of all the compacts increases with increasing sintering temperature, but it remains nearly constant with increasing sintering temperature above 1,200 °C. The tensile strength of the

Fig. 2.13 Comparison of relative sintering density for sintered compacts using alloy and mixed powders

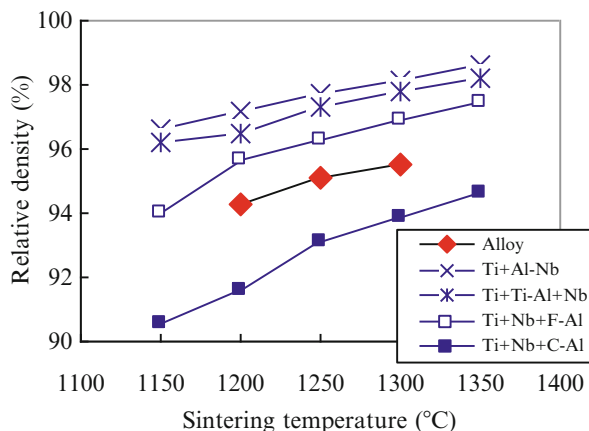


Fig. 2.14 Comparison of oxygen content for sintered compacts using alloy and mixed powders

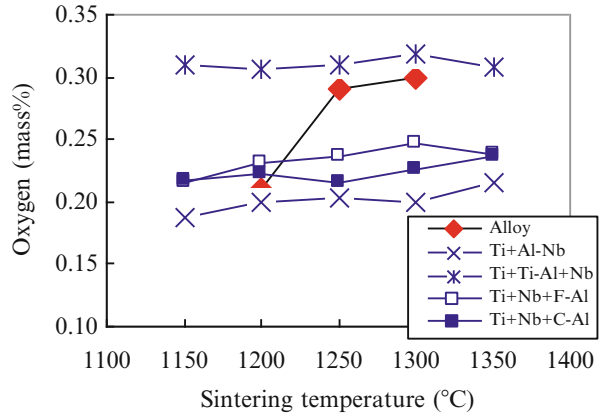


Fig. 2.15 Comparison of carbon content for sintered compacts using alloy and mixed powders

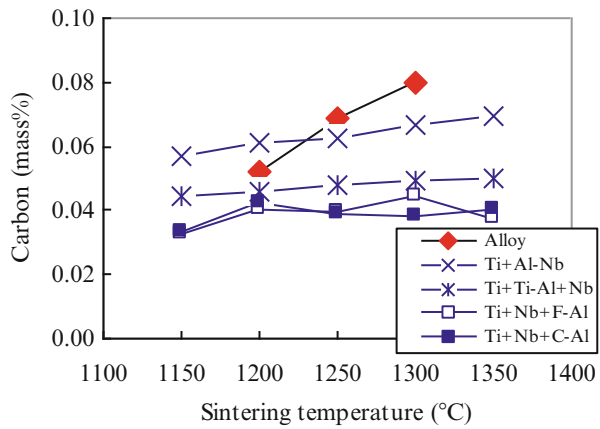


Fig. 2.16 Comparison of tensile strength for sintered compacts using alloy and mixed powders

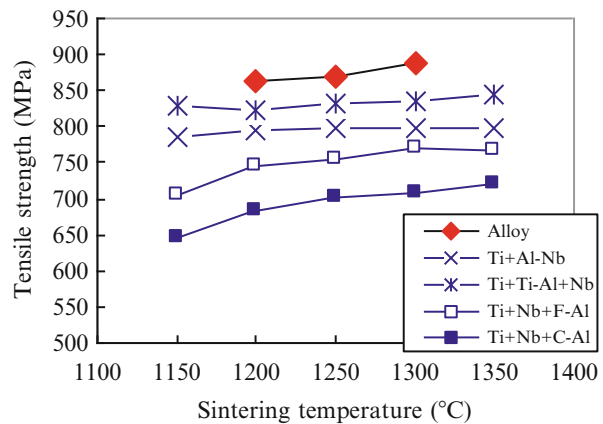
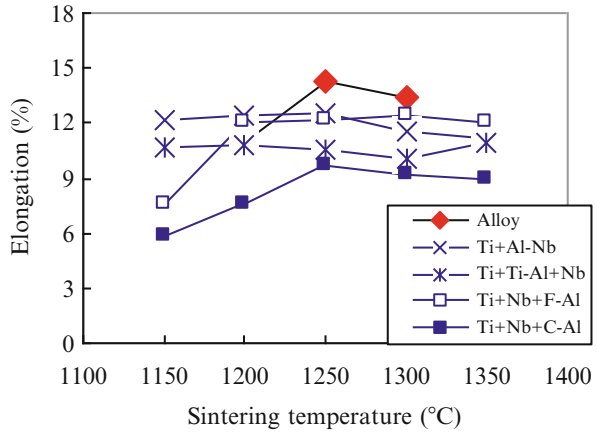


Fig. 2.17 Comparison of elongation for sintered compacts using alloy and mixed powders

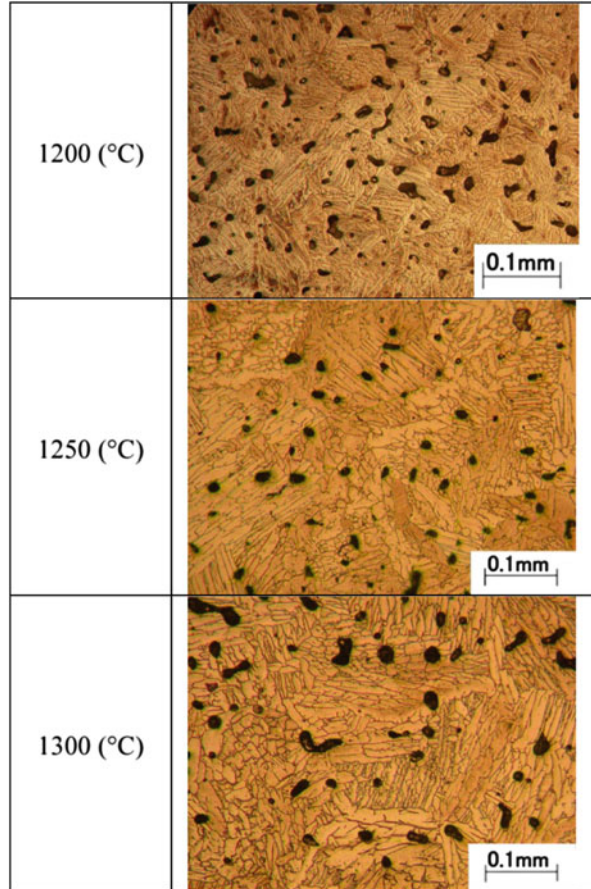


compacts using alloy powder shows the highest value; however, a mixture of Ti, Nb, and coarse Al powders is lower than that of the compacts using other mixtures, even though it increases with increasing sintering temperature. The tensile strength of the compacts using alloy powders is about 100 MPa higher than that of the compacts using a mixture of Ti, Nb, and fine Al powders. Moreover, a compact using alloy powder shows high elongation of above 14 % at the sintering temperature of 1,250 °C.

Figure 2.18 shows the microstructures of Ti-6Al-7Nb alloy compacts sintered at various temperatures. The microstructures of all sintered compacts consist of acicular alpha and intergranular beta phases. The acicular alpha phases become longer and coarser with increasing sintering temperature, which means that the grain size of prior beta was so large for the compacts sintered above 1,250 °C. On the other hand, the sintered compacts using a mixture of Ti, Nb, and coarse Al powders showed many large pores in the microstructure at all sintering temperature. These pores are considered to be the result of the dissolution of Al particles during sintering steps, which also lead to low relative density and poor tensile properties. In the case of the sintered compacts using Ti, Nb, and fine Al powders, although the pores form by dissolution of Al particles during sintering steps similarly, the size of pores is smaller than that of the sintered compacts using a mixture of Ti, Nb, and coarse Al powders due to the small particle diameter of Al powder. Then, it is considered that the compacts using a mixture of Ti, Nb, and fine Al powders have high density and excellent tensile properties at high sintering temperature range.

The relative density, tensile strength, and elongation of the Ti-6Al-7Nb alloy compacts sintered at 1250 °C for 14.4 ks are 97 %, 850 MPa, and 14 %, respectively. These properties are comparable to those of the wrought materials.

Fig. 2.18 SEM micrographs of Ti-6Al-7Nb compact



2.4.2 Summary

The metal injection molding process was applied to produce Ti-6Al-4V and Ti-6Al-7Nb alloy compacts. The sintered compacts show higher density over 95 %. It is important to reduce the oxygen content under 0.35 mass% because the elongation would dramatically decrease from that content.

On the other hand, sintered compacts using Ti-6Al-7Nb alloy powder show relatively higher mechanical properties than the compacts using mixed powder. Eventually, the compacts using alloy powder are improved to be 900 MPa of tensile strength with 15 % of elongation, which are comparable to the properties of wrought materials.

2.5 Fatigue Properties of Ti Alloys Fabricated by MIM

The static mechanical properties of injection molded titanium alloy compacts have been reported so far [19–21]; however, there are few reports regarding the dynamic fracture characteristics [22, 23]. As the dynamic fatigue behavior is of great importance in practical use, fatigue characteristics of injection molded Ti alloy compacts are reviewed.

Usually MIM compacts show higher than 95 % of theoretical density (TD) and sometimes near full density. This leads to higher mechanical properties comparable to wrought materials. However, retained pores (a few percentages) with effect as a notch could be the starting points of crack initiation and may decrease the fatigue limit. Recently hot isostatic pressing (HIP) to MIM compacts is conducted to achieve higher mechanical properties [24]. In order to improve the fatigue limit, HIP is also conducted to injection molded compacts.

Moreover, it has been reported that small additions of Cr or B to Ti alloys produce a reduction of grain size [25, 26] due to the pinning effects against grain growth. Also, certain heat treatments contribute to the grain refinement. Grain refinement is beneficial to the improvement of the tensile strength and ductility. Thus, grain refinement is also expected to improve the fatigue limit.

In this section, rotating bending fatigue characteristics of injection molded pure Ti, Ti-6Al-4V, and Cr or B-added Ti-6Al-4V compacts are investigated using HIP and heat treatment.

2.5.1 Materials

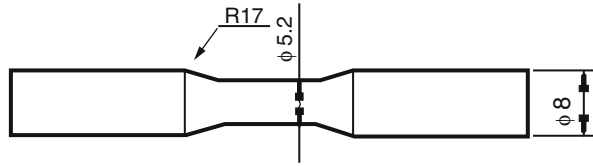
Metal powders used were pure titanium, Ti-6Al-4V alloy, Cr, and TiB₂ powders. Table 2.4 shows the characteristics of powders used. Ti-6Al-4V and Cr powders were mixed to form Ti-6Al-4V-4Cr. Also 0.1 mass% of TiB₂ powder was added to Ti-6Al-4V powder. The fabricated specimens were referred to as Ti, Ti64, Ti64Cr, and Ti64B.

Wax-based binders (paraffin wax 69 mass%, polypropylene 10 mass%, ethylene vinyl acetate 10 mass%, carnauba wax 10 mass %, and di-n-butyl phthalate 1 mass %) were used and mixed with each powder. Powder loading was 65 vol.%.

Table 2.4 Particle diameter and oxygen content of the powders used

Powder	Particle diameter (μm)	Oxygen (mass %)
Pure Ti	32.7	0.170
Ti-6Al-4V	33.0	0.115
Cr	9.90	0.450
TiB ₂	1.28	1.000

Fig. 2.19 Geometry of rotating bending fatigue specimen in mm



2.5.2 Fatigue Testing

Rotating bending fatigue specimens were prepared through an injection molding process. Specimen geometry of the mold is shown in Fig. 2.19. Before thermal debinding, solvent debinding was conducted in vaporous heptane at 58 °C for 4 h. Then the specimens were thermally debound at 600 °C for 2 h in argon and sintered at 1,150–1,350 °C for 2–8 h in high-vacuum atmosphere using a vacuum debinding and sintering furnace (Shimadzu Mectem Inc., Japan, VHSgr 20/20/20). Each specimen was named after the sintering temperature and time used, for example, 1,350–2 means being sintered at 1,350 °C for 2 h. Moreover, heat treatment was conducted for Ti64Cr specimens. Solution heat treatment was performed at 950 °C for 1 h followed by aging at 560 °C for 4 h. Furthermore, HIP (1,150 °C for 1 h) was conducted for Ti64Cr specimens to reduce porosity. For sintered specimens, density measurement, microstructure observation, oxygen and carbon content analysis, and rotating bending fatigue testing were performed.

2.5.3 Results and Discussion

2.5.3.1 Pure Ti

Figure 2.20 shows the relative density of as-sintered unalloyed Ti specimens. The sintered density increased with increasing sintering temperature and time.

Microstructures of the specimens are shown in Fig. 2.21. The number of pores decreased with increasing sintering time, while the pore size seemed to become bigger. As-sintered Ti shows an equiaxed structure, and grain growth was observed with increasing sintering temperature and time.

The oxygen content in the sintered specimens was almost constant, around 0.2 mass%, which was greater than the original oxygen content of the powder but less than 0.33 mass% (at which the elongation dramatically decreases by static tensile testing [27]). The carbon content was around 0.07 mass%, which means that the binder in green specimen was successfully debound.

Figure 2.22 shows the stress amplitude-number of cycles to failure curves obtained by rotating bending fatigue testing. Fatigue limit increased with increasing sintering temperature and time. Fatigue limit of wrought Ti materials by ASTM grade 3 was about 240 MPa. Therefore, the fatigue limit of injection molded Ti shows 64 % of the fatigue limit of wrought Ti.

Fig. 2.20 Relationship between relative sintered density and sintering temperature of Ti specimens

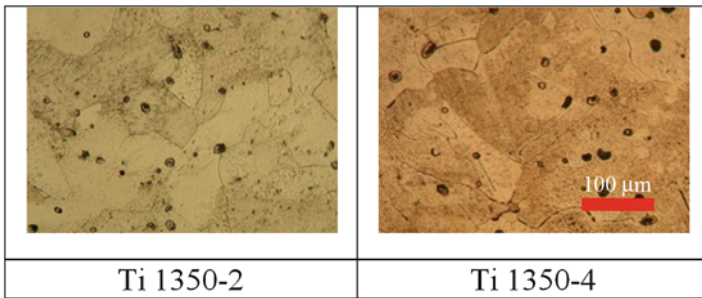
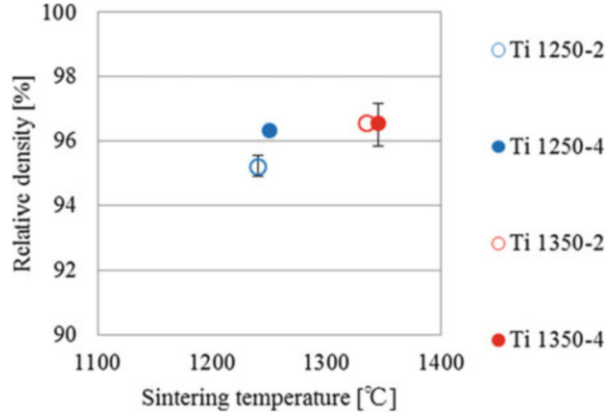


Fig. 2.21 SEM micrographs of Ti specimens

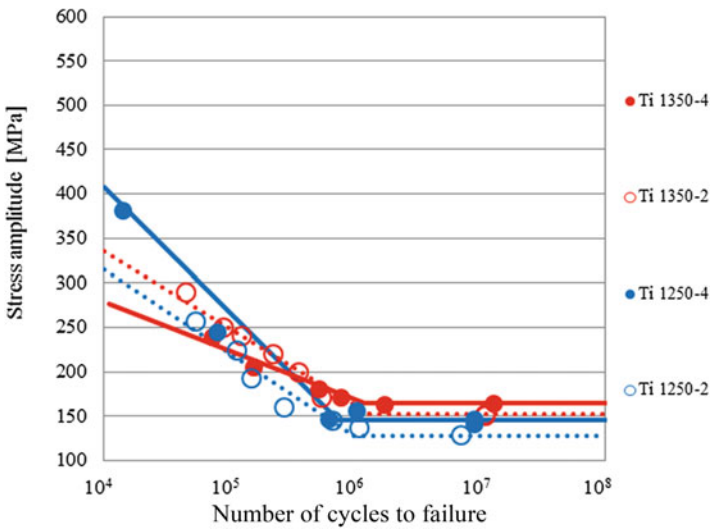


Fig. 2.22 Stress amplitude-number of cycles to failure curves of Ti specimens by rotating bending fatigue testing

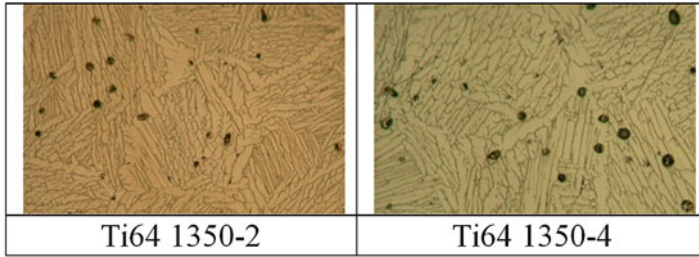
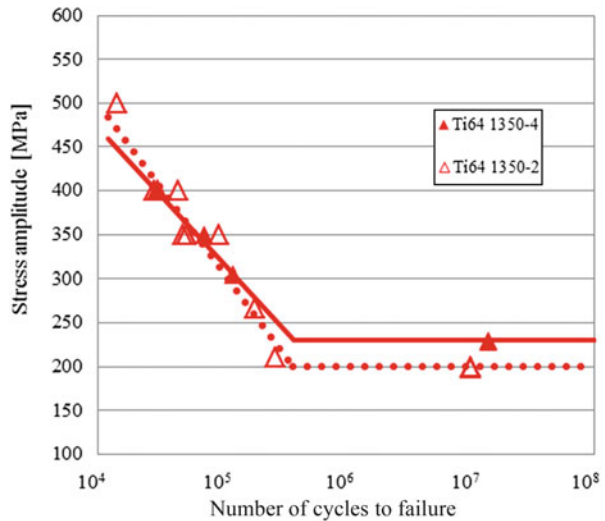


Fig. 2.23 SEM micrographs of Ti64 specimens

Fig. 2.24 Stress amplitude -number of cycles to failure curves Ti64 specimens by rotating bending fatigue testing



2.5.3.2 Ti-6Al-4V

Sintered densities of the specimens were around 97.5 %. Their microstructures are shown in Fig. 2.23. Pore size seemed to become bigger with increasing sintering time. Ti64 showed the α - and β -lamellar structure. The lamellar structure formed in each prior β -grain, and the prior β -grain size increased with increasing sintering time. Similarly, the oxygen content in the as-sintered specimens was almost constant, below 0.3 mass%. The carbon content was less than 0.1 mass%.

Figure 2.24 shows the stress amplitude-number of cycles to failure curves obtained by rotating bending fatigue testing. Fatigue limit increased with increasing sintering time. The fatigue limit of wrought Ti64 by ASTM grade 5 was 510 MPa. In this case, the fatigue limit of injection molded Ti64 shows 45 % of the fatigue limit of the wrought Ti64, which is very low.

2.5.3.3 Ti-6Al-4V-4Cr

Figure 2.25 shows the sintered density of each specimen, which increased with increasing sintering temperature. Specimens except Ti64Cr 1150–8 showed higher than 96 %TD. Also the specimen treated by HIP showed a relative density over 99 %TD.

The microstructures of the specimens are shown in Fig. 2.26. The number of pores decreased with increasing sintering temperature. A few pores remained even after HIP, and their pore diameter is around 20 μm . HIP can reduce the number of pores; however, it cannot eliminate all pores. Ti64Cr also showed the α - and β -lamellar structure. The prior β -grain size increased with increasing sintering temperature. The oxygen content in the specimens was little changed, below 0.3 mass%. The carbon content was below 0.09 mass%.

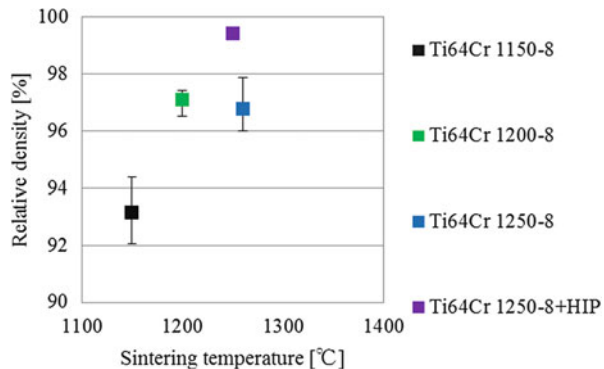
Figure 2.27 shows the stress amplitude-number to failure curves of specimens obtained by rotating bending fatigue testing. Fatigue limit increased with increasing sintering temperature. The specimens treated by HT and HIP showed much higher fatigue limit.

2.5.3.4 Ti-6Al-4V-0.03B

The sintered density obtained was around 97 %TD. The resulting α - and β -lamellar structure is shown in Fig. 2.28. The oxygen content in Ti64B was measured to 0.37 mass%, which is higher than the oxygen content of other specimens because of the higher oxygen content of the original TiB₂ powder (1 mass%) introduced.

Figure 2.29 shows the stress amplitude-number of cycles to failure curves obtained by rotating bending fatigue testing. Fatigue limit (fatigue limit at 10⁷ cycles) is around 360 MPa.

Fig. 2.25 Relationship between relative sintered density and sintering temperature of Ti64Cr specimens



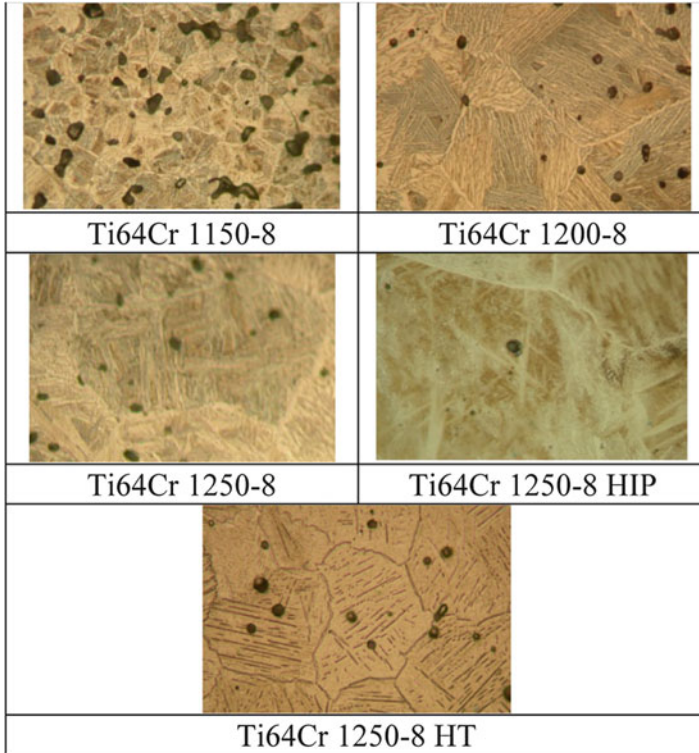


Fig. 2.26 SEM micrographs of various Ti64Cr specimens

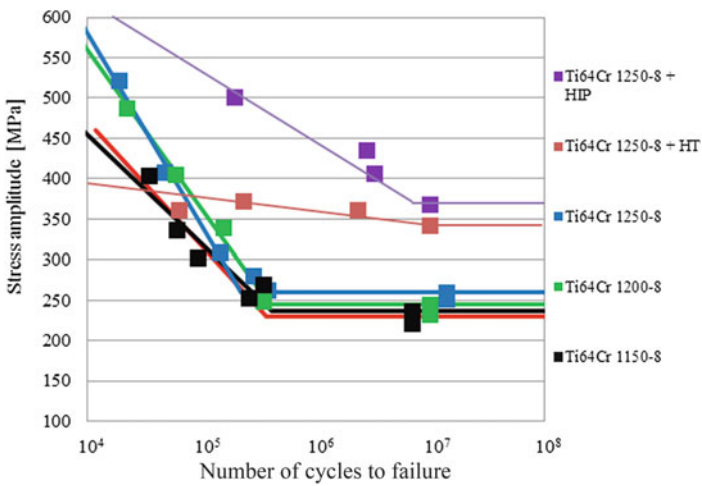


Fig. 2.27 Stress-number curves of Ti64Cr specimens by rotating bending fatigue testing

Fig. 2.28 SEM micrograph of Ti64B specimen

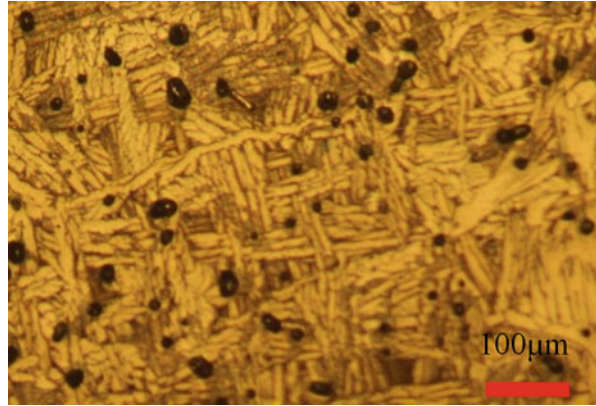
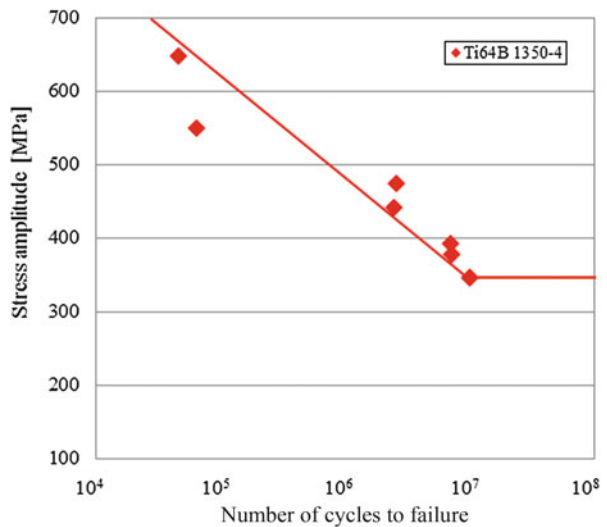


Fig. 2.29 Stress amplitude-number of cycles to failure curves of Ti64B specimens by rotating bending fatigue testing



2.5.3.5 Discussion

The sintered densities of all specimens are summarized in Fig. 2.30. They are around 97 %TD. From the microstructure, the α -lamellae in Ti64Cr are thinner than that in Ti64. Thus, the addition of Cr powder refined the microstructure. Moreover, Ti64B shows smaller prior β -grain size than that of Ti64. Finer grain size is also effective to improve the fatigue properties. Figure 2.31 shows the relationship between the grain size and sintering temperature. Grain size increased with increasing sintering temperature and time. Although the grain size of Ti64Cr was smaller than that of Ti64, the grain size of Ti64Cr 1250–8 after HIP became larger. On the other hand, certain heat treatment conditions could change the smaller size. In spite of the higher sintering temperature used, the grain growth of Ti64B seemed to be negligible.

Fig. 2.30 Relationship between relative density and sintering temperature for various specimens

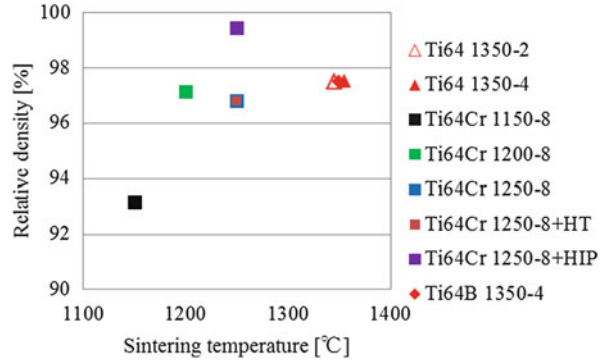
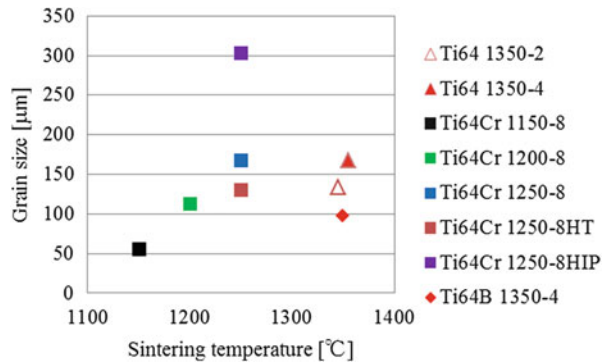


Fig. 2.31 Relationship between grain size and sintering temperature for various specimens



The fatigue limit of Ti showed 64 % that of the wrought Ti, while Ti64 showed only 45 % that of the wrought Ti64. It is known that, in harder materials, high notch sensitivity causes the decrease of fatigue limit. The notch sensitivity should become higher for Ti64, which showed lower fatigue limit.

The fatigue limits of all specimens are summarized in Fig. 2.32. Ti64Cr shows 30 MPa higher fatigue limit than that of Ti64, because of the refinement of α -lamellae. Ti64Cr HT shows 100 MPa higher fatigue limit than that of Ti64Cr. Ti64Cr HIP and Ti64B show 55 % improvement in fatigue limit compared to the wrought Ti64; however, they are still weaker than that of the wrought Ti64.

Fatigue ratio is the ratio of fatigue limit to tensile strength. The fatigue ratios of all specimens are shown in Fig. 2.33. The fatigue ratio of wrought Ti materials is around 0.4–0.6, while that of P/M material is usually around 0.3 [28]. From Fig. 2.33, the fatigue ratio of injection molded Ti alloy specimens is around 0.3, including HT- and HIP-treated specimens. Although the microstructural refinement is effective to improve the fatigue limit, the results suggest that even a small amount of remained pores could cause a significant decrease in fatigue limit.

In order to clarify the effect of retained pores on the fracture behavior such as fatigue crack propagation, in situ replica observations were performed. At certain cycles, the rotating was terminated and the surfaces of specimens were replicated using acetyl cellulose film and methyl acetate. Figure 2.34 shows the photograph of

Fig. 2.32 Relationship between fatigue limit and sintering temperature

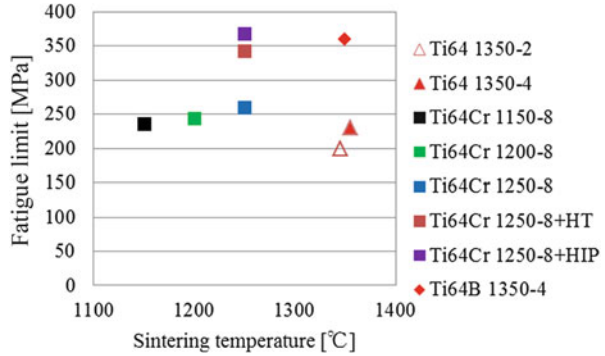


Fig. 2.33 Relationship between fatigue limit and tensile strength (fatigue ratio)

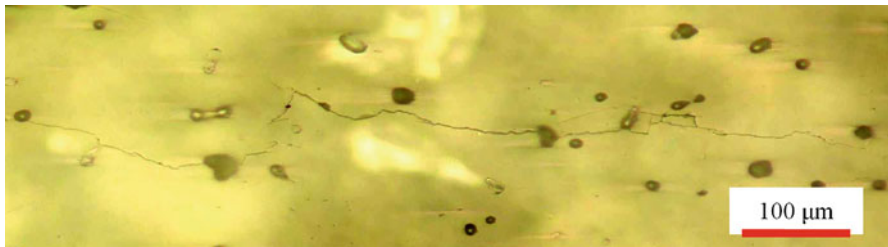
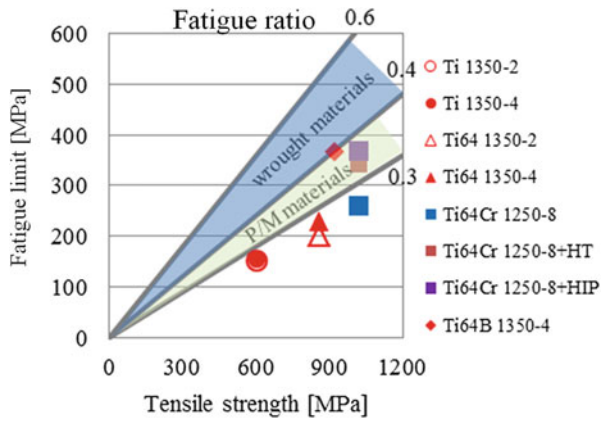


Fig. 2.34 Surface crack by replica observation of Ti64Cr specimen at 80 % of fatigue life

a replica film for Ti64Cr. It was taken at 80 % of fatigue life. There is an 800 μm long crack on the surface of the specimen. Fatigue cracks started from several pores and connected each other, resulting in a longer crack.

Figure 2.35 shows the etched microstructure of the surface of the specimen after fatigue tests to reveal the crack propagation root. Two types of crack propagation were observed: one is transgranular fracture, and the other is intergranular fracture. Normally, a crack that occurred in the wrought materials starts from slipping inside

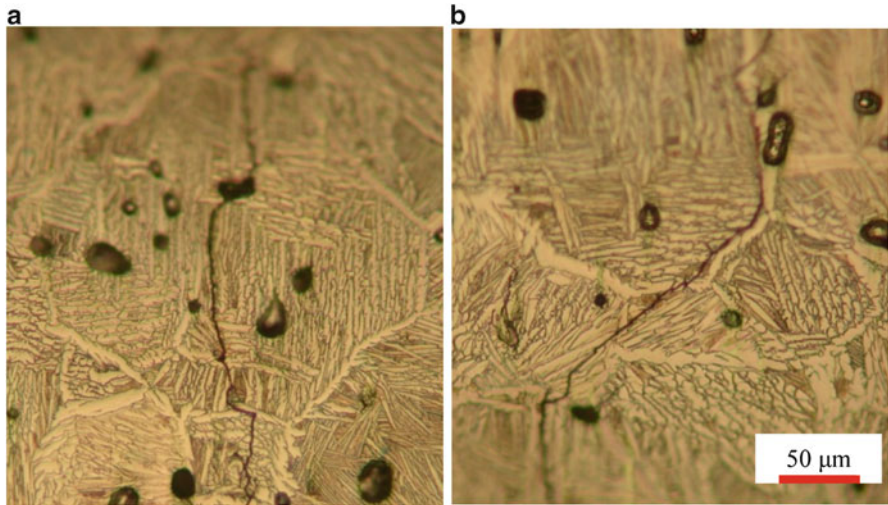


Fig. 2.35 Crack propagation behavior of Ti64Cr specimen. (a) Transgranular fracture, (b) intergranular fracture

the grain, and then the crack goes along the grain boundary [29]. Crack initiation in the sintered materials occurs differently. They start at pores in a grain or at the grain boundary and then propagate easily to the next pores or along the grain boundary. This causes the lower fatigue limit of the as-sintered specimens.

2.5.4 Summary

In this section, the fatigue properties of the injection molded Ti, Ti-6Al-4V, Ti-6Al-4V-4Cr, and Ti-6Al-4V-0.03B were reviewed. Fatigue limit of pure Ti shows 64 % of the fatigue limit of the wrought material, while Ti64 shows only about 45 %. The high notch sensitivity causes the decrease of fatigue limit of Ti64. By addition of Cr or TiB₂, the fatigue limits of Ti64Cr and Ti64B are higher than that of Ti64 because of the microstructural refinement, especially the α - and β -lamellae. Fracture of injection molded specimens was confirmed by in situ observation, in which the crack initiated from the pores on the surface of the specimen and propagated easily by connecting the pores. HIP treatment improved the fatigue limit because of the further densification; however, a few pores still remained in the matrix which facilitated the crack generation, resulting in still not high fatigue limit.

2.6 Conclusion

Complex-shaped component can be obtained through the powder metallurgy processing route. Especially, metal injection molding (MIM) process is an advanced net-shape processing technique for the mass production of complex-shaped components. This technology also reduces the production cost. Sintered compacts obtained by MIM process show high relative density over 95 % and excellent mechanical properties. MIM process is a suitable technique for titanium and its alloys to reduce the processing cost and material cost.

In this chapter, the tensile and fatigue properties of Ti, Ti-6Al-4V, Ti-6Al-4V-4Cr, Ti-6Al-4V-0.03B, and Ti-6Al-7Nb were reviewed. The sintered compacts showed higher density over 95 %. It was important to reduce the oxygen content under 0.35 mass% because the elongation would dramatically decrease from that content. Sintered compacts using Ti-6Al-7Nb alloy powder showed 900 MPa of tensile strength with 15 % of elongation, which were comparable to the properties of wrought materials. Fatigue limit of pure Ti showed 64 % the fatigue limit of wrought material, while Ti-6Al-4V showed only about 45 %. The high notch sensitivity caused the decrease of fatigue limit of Ti-6Al-4V. By addition of Cr or TiB₂, the fatigue limits of Ti-6Al-4V-4Cr and Ti-6Al-4V-0.03B were higher than that of Ti-6Al-4V because of the microstructural refinement, especially the α - and β -lamellae. HIP treatment improved the fatigue limit because of the further densification; however, a few pores still remained in the matrix which facilitated the crack generation, resulting in still not high fatigue limit. MIM of titanium alloy is still a novel process and under continuous development.

Acknowledgments The authors would like to express sincere thanks to Osaka Titanium Technologies Co., Ltd., for supplying titanium powders.

References

1. German RM, Bose A (1997) Injection molding of metals and ceramics. Metal Powder Industries Federation, Princeton
2. Miura H, Takagi K (1996) Powder Metallurgy Science, Uchida Rokakuho, Tokyo
3. Japan Powder Metallurgy Association (2013) <http://www.jpma.gr.jp/index.html>. Accessed 28 Dec 2013
4. Omar MA, Mustapha M, Ali EAGE, Subuki I, Meh B (2010) Production of medical device using MIM technique. AIP Conf Proc 1217:287–293
5. Fraunhofer Institute for Manufacturing Technology and Advanced Materials (2013) http://www.ifam.fraunhofer.de/en/Bremen/Formgebung_Funktionswerkstoffe/Pulvertechnologie/Projekte/Herzklappen.html. Accessed 28 Dec 2013
6. Ebel T (2008) Titanium and titanium alloys for medical applications: opportunities and challenges. PIM Int 2(2):21–30
7. German RM (2011) Markets, applications, and financial aspects of global metal powder injection molding (MIM) technologies. Proc PowderMet 2011, 04-120-133

8. Heaney DF (2012) Handbook of metal injection molding. Woodhead Publishing in Materials, Cambridge
9. Itoh Y, Harikou T, Sato K, Miura H (2004) Improvement of ductility for injection moulded Ti-6Al-4V alloy. In: Proceedings of 2004 powder metallurgy world congress (PM 2004), compiled by Danninger H, Ratzl R, vol 4. European Powder Metallurgy Association, Vienna, Austria, pp 445–450
10. Itoh Y, Harikou T, Sato K, Miura H (2005) Fabrication of near- α titanium alloy by metal injection molding. *J Jpn Soc Powder Powder Metall* 52:43–48
11. Itoh Y, Miura H, Sato K, Niinomi M (2007) Effect of mixed powders on the properties of Ti-6Al-7Nb alloy by metal injection molding. *Mater Sci Forum* 534–536:357–360
12. Itoh Y, Harikou T, Sato K, Komatsu T (2005) Method of preparations for sintered titanium alloy compacts by metal injection molding. JPN Patent No. 2005–281736, Oct 13, 2005
13. Itoh Y, Harikou T, Satoh K, Miura H (2002) Development of the binder systems for solvent and thermal debinding in MIM process. *J Jap Soc Powder Powder Metall* 49:518–521
14. Itoh Y, Miura H, Toshiaki U, Sato K (2010) The influence of density and oxygen content on the mechanical properties of injection molded Ti-6Al-4V alloys. *Adv Powder Metall Particle Mater* 1:4.46–4.53
15. Uematsu T, Itoh Y, Sato K, Miura H (2006) Effects of substrate for sintering on the mechanical properties of injection molded Ti-6Al-4V alloy. *J Jpn Soc Powder Powder Metall* 53:755–759
16. Miura H, Takemasu T, Kuwano Y, Itoh Y, Sato K (2006) Sintering behavior and mechanical properties of injection molded Ti-6Al-4V alloys. *J Jpn Soc Powder Powder Metall* 53:815–820
17. Arimoto N, Fujita M, Nishioka K, Miura H (2007) New production method by gas-atomized process of titanium alloy powder. Ti-2007 science and technology, compiled by Niinomi M, Akiyama S, Ikeda M, Hagiwara M, Maruyama K, vol 2. The Japan Institute of Metals, Kyoto, pp 1137–1140
18. Itoh Y, Uematsu T, Sato K, Miura H (2008) Effect of Al-40V alloy powders on the properties of injection molded Ti-6Al-4V alloys. *J Jpn Soc Powder Powder Metall* 55:666–670
19. Osada T, Miura H, Itoh Y, Fujita M, Arimoto N (2008) Optimization of MIM process for Ti-6Al-7Nb alloy powder. *J Jpn Soc Powder Powder Metall* 55(10):726–731
20. Itoh Y, Miura H, Uematsu T, Sato K (2009) Advanced MIM process for high performance Ti alloy materials. *J Solid Mech Mater Eng* 3(12):1297–1305
21. Itoh Y, Miura H, Uematsu T, Sato K, Niinomi M (2007) Improvement of the properties of Ti-6Al-7Nb alloy by metal injection molding. *Adv Powder Metall Particle Mater Part* 4:81–86
22. Ferri OM, Ebel T, Bormann R (2009) High cycle fatigue behaviour of Ti-6Al-4V fabricated by metal injection moulding technology. *Mater Sci Eng A* 504:107–113
23. Osada T, Noda M, Kang H, Tsumori F, Miura H (2012) Dynamic fracture characteristics of injection molded titanium alloy compacts. *Int Conf Mater Process Technol* 2012:141–146
24. Huang WY, Da Chen C, Chen YN, Shih WJ, Chang CH (2012) Defect detection of metal injection modeling by micro computed tomography. *Appl Mech Mater* 229–231:1445–1448
25. Itoh Y, Miura H, Uematsu T, Osada T, Sato K (2009) Effect of Fe or Cr addition on the strengthening Ti-6Al-4V alloy by metal injection molding. *J Solid Mech Mater Eng* 3(6):921–930
26. Hagiwara M, Kitaura T, Ono Y, Yuri T, Ogata T, Kanou O (2012) High cycle fatigue properties of a minor boron-modified Ti6Al4V alloy. *Mater Trans* 53(8):1486–1494
27. Itoh Y, Uematsu T, Sato K, Miura H (2009) Effect of oxygen content and relative density on the tensile properties of injection molded Ti-6Al-4V alloy. *J Jpn Soc Powder Powder Metall* 56(5):259–263
28. Hasegawa M (1973) Stainless steel handbook. Nikkan Kogyo Shimbun Ltd, Tokyo
29. Akahori T, Niinomi M, Ozeki A (1998) Effect of microstructure on small fatigue crack initiation and propagation characteristics of Ti-6Al-7Nb alloy. *J Jpn Inst Metals* 62(10):952–960